

Geochemical Processes During Managed Aquifer Recharge With Desalinated Seawater

Ganot, Y., Holtzman, R., Weisbrod, N., Russak, A., Katz, Y. & Kurtzman, D.

Author post-print (accepted) deposited by Coventry University's Repository

Original citation & hyperlink:

Ganot, Y, Holtzman, R, Weisbrod, N, Russak, A, Katz, Y & Kurtzman, D 2018, 'Geochemical Processes During Managed Aquifer Recharge With Desalinated Seawater', *Water Resources Research*, vol. 54, no. 2, pp. 978-994.
<https://dx.doi.org/10.1002/2017WR021798>

DOI 10.1002/2017WR021798

ISSN 0043-1397

ESSN 1944-7973

Publisher: American Geophysical Union (AGU)




Accepted for publication in *Water Resources Research*. Copyright (2018) American Geophysical Union. Further reproduction or electronic distribution is not permitted.

**"Ganot, Y, Holtzman, R, Weisbrod, N, Russak, A, Katz, Y & Kurtzman, (2018), Title of article, 'Geochemical Processes During Managed Aquifer Recharge With Desalinated Seawater', *Water Resources Research*, vol. 54, no. 2, pp. 978-994.
<https://dx.doi.org/10.1002/2017WR021798>To view the published open abstract, go to <https://dx.doi.org/10.1002/2017WR021798>**

Copyright © and Moral Rights are retained by the author(s) and/ or other copyright owners. A copy can be downloaded for personal non-commercial research or study, without prior permission or charge. This item cannot be reproduced or quoted extensively from without first obtaining permission in writing from the copyright holder(s). The content must not be changed in any way or sold commercially in any format or medium without the formal permission of the copyright holders.

This document is the author's post-print version, incorporating any revisions agreed during the peer-review process. Some differences between the published version and this version may remain and you are advised to consult the published version if you wish to cite from it.

Geochemical processes during managed aquifer recharge with desalinated seawater

Y. Ganot^{1,2} , R. Holtzman² , N. Weisbrod³ , A. Russak³, Y. Katz⁴ and D. Kurtzman¹

¹Institute of Soil, Water and Environmental Sciences, The Volcani Center, Agricultural Research Organization, Rishon LeZion, 7528809, Israel

²Hydrology and Water Resources, The Hebrew University of Jerusalem, Rehovot, 7610001, Israel

³Department of Environmental Hydrology & Microbiology, Zuckerberg Institute for Water Research, Jacob Blaustein Institutes for Desert Research, Ben-Gurion University of the Negev, Midreshet Ben-Gurion, 8499000, Israel

⁴Mekorot, Water Company Ltd, Tel Aviv, 6713402, Israel

Corresponding author: Yonatan Ganot (yonatan.ganot@mail.huji.ac.il)

Key Points:

- Ion enrichment of Mg^{2+} , Na^+ , Ca^{2+} and HCO_3^- was observed along the vadose zone during managed aquifer recharge with desalinated seawater
- Field sampling of sediment and water were used to calibrate a reactive transport model of cation exchange and calcite dissolution
- Simulations suggest that infiltration can serve as an alternative post-treatment for remineralization of Ca^{2+} , HCO_3^- and partly for Mg^{2+}

This article has been accepted for publication and undergone full peer review but has not been through the copyediting, typesetting, pagination and proofreading process which may lead to differences between this version and the Version of Record. Please cite this article as an 'Accepted Article', doi: 10.1002/2017WR021798

Abstract

We study geochemical processes along the variably-saturated zone during managed aquifer recharge (MAR) with reverse-osmosis desalinated seawater (DSW). The DSW, post-treated at the desalination plant by calcite dissolution (remineralization) to meet the Israeli water quality standards, is recharged into the Israeli Coastal Aquifer through an infiltration pond. Water quality monitoring during two MAR events using suction cups and wells inside the pond, indicates that cation exchange is the dominant subsurface reaction, driven by the high Ca^{2+} concentration in the post-treated DSW. Stable isotope analysis shows that the shallow groundwater composition is similar to the recharged DSW, except for enrichment of Mg^{2+} , Na^+ , Ca^{2+} and HCO_3^- . A calibrated variably-saturated reactive transport model is used to predict the geochemical evolution during 50 years of MAR for two water quality scenarios: (i) post-treated DSW (current practice); and (ii) soft DSW (lacking the remineralization post-treatment process). The latter scenario was aimed to test soil-aquifer-treatment (SAT) as an alternative post-treatment technique. Both scenarios provide an enrichment of $\sim 2.5 \text{ mg L}^{-1}$ in Mg^{2+} due to cation-exchange, compared to practically zero Mg^{2+} currently found in the Israeli DSW. Simulations of the alternative SAT scenario provide Ca^{2+} and HCO_3^- remineralization due to calcite dissolution at levels that meet the Israeli standard for DSW. The simulated calcite content reduction in the sediments below the infiltration pond after 50 years of MAR was low ($< 1\%$). Our findings suggest that remineralization using SAT for DSW is a potentially sustainable practice at MAR sites overlying calcareous sandy aquifers.

1 Introduction

The growing use of desalinated seawater (DSW) as a viable water source [Gude, 2016], includes its integration in various downstream water systems such as reservoirs, wastewater treatment plants and agricultural irrigation [Birnhack *et al.*, 2011]. Recently, reverse-osmosis DSW has also been used as a source for managed aquifer recharge (MAR) in the Israeli Coastal Aquifer using an infiltration pond [Ganot *et al.*, 2017]. MAR is a water management practice in which excess water is stored in aquifer for future consumption [Dillon, 2005]. Despite the growing use of DSW as a water source, there are few published works on MAR with DSW (mainly from the arid Arabian Gulf region).

Injection of DSW into wells was conducted in Kuwait during 1970–1990 to evaluate the feasibility of MAR with DSW into a brackish aquifer. Well clogging was identified as a major concern, especially in clastic aquifers [Mukhopadhyay *et al.*, 1994]. Further laboratory core-flow and batch experiments indicated permeability reduction, which was explained by clogging with fines originated from carbonates and evaporites dissolution. Yet, from these works it was concluded that MAR with DSW is feasible in the studied geological formations [Al-Awadi *et al.*, 1995; Mukhopadhyay *et al.*, 1998, 2004].

MAR with reverse-osmosis-treated wastewater (not DSW) was studied at the St-André MAR site, Belgium (recharge of $\sim 2 \cdot 10^6$ m³ per year), using flow and transport modeling [Vandenbohede *et al.*, 2008, 2009a; Vandenbohede and Van Houtte, 2012], isotope and geochemical analysis [Kloppmann *et al.*, 2008b; Vandenbohede *et al.*, 2009b] and reactive transport modeling [Vandenbohede *et al.*, 2013]. Carbonate dissolution was found to be the main geochemical process at St-André site, due to the low total dissolved solids (TDS) of the infiltrating water (< 50 mg L⁻¹), while cation exchange being of secondary importance.

Recently, Stuyfzand *et al.* [2017] reported on water quality changes of DSW during trial infiltration runs at Liwa MAR site, Abu Dhabi. Water quality changes include small TDS increase by dissolution of SiO₂, K-feldspar and dolomite; cation exchange of Ca²⁺/Na⁺, and mobilization of trace elements. Based on observations and modeling results the authors concluded that the recovered water meets the Abu Dhabi drinking water standards.

Here, we study the geochemical processes during pond-infiltration MAR with post-treated, reverse-osmosis DSW into a calcareous sandy aquifer with a 25m-thick unsaturated zone. The DSW composition (e.g. high $\text{Ca}^{2+}/\text{Mg}^{2+}$ [Ronen-Eliraz *et al.*, 2017]) together with the relatively thick unsaturated zone creates unique conditions which distinguish this MAR site from other sites. Moreover, we use unsaturated zone and shallow groundwater field-data to calibrate a mechanistic reactive transport model including cation exchange and calcite dissolution. The model is then used for testing soil-aquifer-treatment (SAT) as an alternative to the industrial post-treatment techniques for remineralization of soft DSW [Birnhack *et al.*, 2011]. We hypothesize that we can use the calcareous sandstone aquifer as a mineral source for remineralization of soft DSW through calcite dissolution and cation exchange. Our results suggest an alternative, sustainable management practice for DSW remineralization in MAR sites overlying calcareous sandy aquifers.

The paper is organized as follows: we begin by presenting field data from both the unsaturated and saturated zones that captures the main geochemical processes. Next, the calibration of a variably-saturated reactive transport model is described. Finally, we provide predictions of two scenarios of long-term MAR with DSW—with and without post-treatment—and discuss their implications.

2 Study site

The study site is located on sand dunes 28 m above mean sea level (AMSL), above the northern part of the Israeli Coastal Aquifer (Figure 1a). Below the site, the aquifer thickness is ~80 m, composed mainly of sand, calcareous sandstone (Kurkar hereafter) and clay lenses. The local climate is Mediterranean, with annual average temperature of 20.2°C, and annual mean precipitation of 566 mm/yr [Israel Meteorological Service, 2016]. The MAR site includes a settling pond and three infiltration ponds that capture the natural ephemeral flows from the Menashe-Hills streams. About 30 production wells were installed around the ponds to recover the recharged water from the aquifer [Sellinger and Aberbach, 1973]. Regional groundwater level is ~25 m below ground surface (September 2014, [Israel Hydrological Service, 2014]) and the characteristic aquifer properties are: hydraulic conductivity of 10 m/d, storativity of 0.25 and porosity of 0.4 [Shavit and Furman, 2001]. The geochemical state of the upper aquifer is oxic,

while reductive conditions occur only in deep parts of the aquifer, which are beyond the scope of this study [Levy *et al.*, 2017].

In the last few years, surplus of DSW from the Hadera reverse-osmosis desalination plant, are diverted to the southern infiltration pond (Figure 1b). The Hadera desalination plant, located 4 km west of the infiltration ponds, started to operate in 2010, and it is one of five large seawater-desalination plants (production capacity $\geq 90 \cdot 10^6 \text{ m}^3$ per year per plant) established on the Mediterranean coast of Israel during 2005–2015 [Stanhill *et al.*, 2015]. The desalinated seawater is usually distributed directly to consumers through the national water grid. However, in operational situations in which large volumes ($>10^5 \text{ m}^3$) of desalinated seawater cannot be distributed immediately, the expensive surplus DSW is stored through MAR operations [Ronen-Eliraz *et al.*, 2017; Ganot *et al.*, 2017].

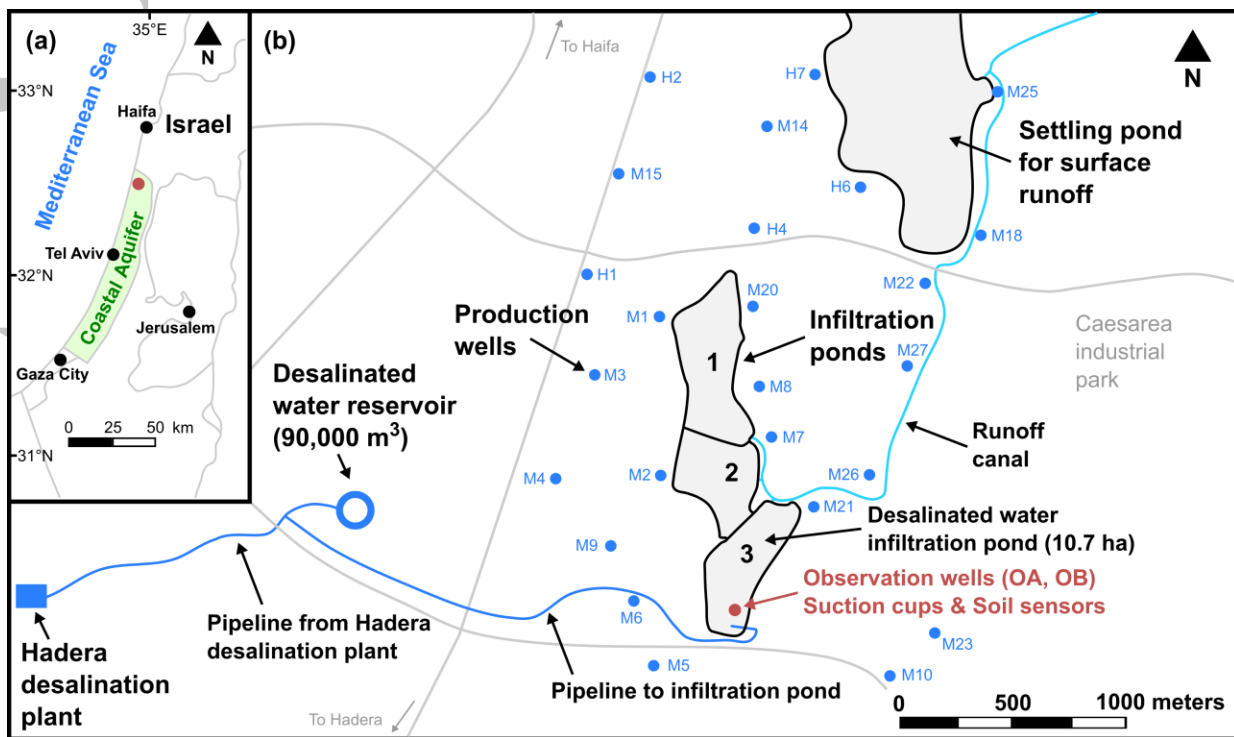


Figure 1. (a) Location of the Israeli Coastal Aquifer and the Menashe MAR site (red circle). (b) The Menashe MAR site. Surplus of desalinated seawater is delivered from Hadera desalination plant (lower left) to the southern infiltration basin (pond 3) where recharge is monitored by observation wells, suction cups, and soil sensors.

3 Field data

3.1 Sampling

A dedicated monitoring system was installed in order to study the hydrological and geochemical processes during MAR with DSW. For further details of the hydrological monitoring and flow model of the MAR events, see *Ganot et al.* [2017]. Silicon-carbide suction cups (SIC20, UMS) installed at depths of 0.5, 1, 2 and 3 m below the pond surface, were used for pore-water sampling at the beginning and end of the infiltration events. Two groundwater observation wells (OA and OB; Figure 1b) were used for groundwater sampling. The observation wells are 30 m deep, perforated at the lower part of the well (10 m from the bottom) and penetrating the saturated zone. Pressure and electrical conductivity (EC) were measured continuously in the observation wells, while water was sampled at the beginning and end of the MAR events and regularly every 3 months. DSW was sampled at the inlet pipe to the infiltration pond during MAR events. Sediment samples were taken from auger during the drilling of the observation wells for analysis of cation exchange capacity (CEC), adsorbed cations and carbonate content.

3.2 Analytical methods

Water samples were analyzed for cations by inductively coupled plasma optical emission spectrometer (ICP-OES, 720-ES, Varian), anions by ion chromatography (ICS-5000, Dionex), bicarbonate by titration with HCl and stable water isotopes by CRDS analyzer (L2130-i, Picarro). CEC and adsorbed cations were determined by the ammonium acetate method [*Sumner and Miller, 1996*], with sodium analyzed by flame photometer (Sherwood M410, Sherwood Scientific Ltd) and adsorbed cations by ICP-OES. Sediment carbonate content was determined by the pressure calcimeter method [*Loeppert and Suarez, 1996*].

3.3 Observations

The lithologic profiles of observation wells OA and OB (8 m apart) are relatively similar [*Ganot et al., 2017*]. The top 30 m of sediments consist of two recurring sequences that include a sand layer overlaying a sandy-clay-loam bed, down to a depth of ~15 m. Below these sequences, Kurkar dominates, alternating with lenses of sandy loam. Carbonate content in the top sand layer (0–4 m depth) is 8%, up to 50% in the Kurkar layer (17–30 m depth), and lower than 2%

elsewhere. The exchangeable cations are dominated by Ca^{2+} , followed by Mg^{2+} , Na^+ and K^+ (in decreasing order), with the exception of the top sand layer with Mg^{2+} , Ca^{2+} , K^+ and Na^+ (Figure 2). The typical mineralogical composition of the sediments in the northern Israeli Coastal Aquifer is dominated by quartz, secondary calcite, and traces of aragonite, feldspars, and phyllosilicates. Organic matter is $\sim 0.5\%$ [Russak and Sivan, 2010].

Two MAR events, during January 2015 and January-February 2016, are studied in this work. A volume of $2.45 \cdot 10^6 \text{ m}^3$ DSW was continuously discharged during January 2015, whereas $1.3 \cdot 10^6 \text{ m}^3$ DSW was discharged in three periods during January-February 2016 (Figure 3a). These relatively high discharge volumes of DSW during short duration result in substantial rise of groundwater levels (up to 17 m) below the infiltration pond and a general decrease of the groundwater EC (Figure 3b).

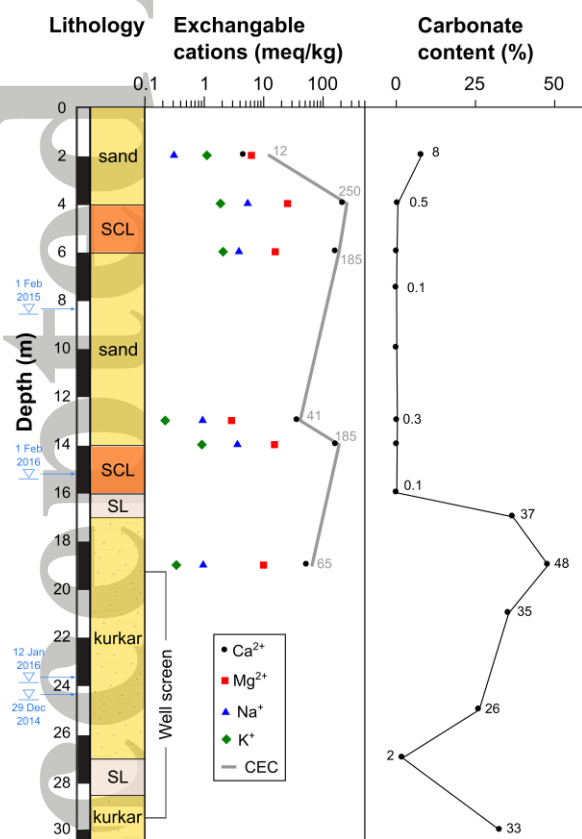


Figure 2. Depth profiles (0 m is pond ground surface): sediments of observation well OA (SCL – sandy clay loam, SL – sandy loam, Kurkar – local calcareous sandstone), exchangeable cations (Ca^{2+} , Mg^{2+} , Na^+ , K^+), cation exchange capacity (CEC) and carbonate content. Sediment samples were obtained in 2014 before the studied MAR events. The well screen and water levels before and after the MAR events are shown for reference.

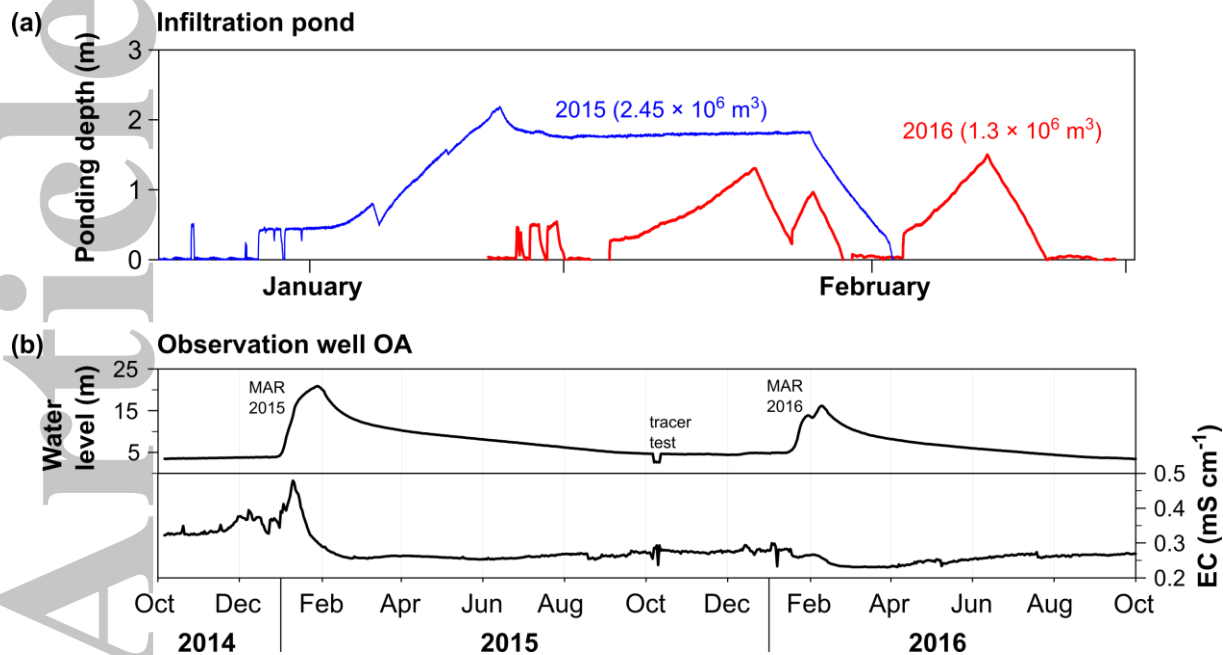


Figure 3. (a) Ponding depth during 2015 and 2016 MAR events. (b) Groundwater level (AMSL) and electric conductivity (EC) at observation well OA.

The concentration of the major ions (excluding K^+ that was always lower than 0.04 meq L^{-1}) obtained from the suction-cups in the shallow unsaturated zone (0 to 3 m) before and after the MAR events shows some variability compared to the DSW inlet source water (indicated as 0 m depth; Figure 4a). Some increase in $[\text{Cl}^-]$ (where $[\text{X}]$ is the concentration of ion X, hereafter) and to a lesser extent in $[\text{Na}^+]$ is observed along the profile (especially on 12 January 2016), but most prominent is the increase in $[\text{Mg}^{2+}]$ associated with a decrease in $[\text{Ca}^{2+}]$. Plotting the difference in ion concentration at the unsaturated zone compared to the concentration in DSW (i.e., $\Delta[\text{X}] = [\text{X}]_z - [\text{X}]_{\text{DSW}}$, where the subscript z is the suction-cup depth) shows clearly that the enrichment of $[\text{Mg}^{2+}]$ is accompanied by a depletion in $[\text{Ca}^{2+}]$ (Figure 4b). Hence, it is assumed that this process is controlled by cation exchange (i.e., Ca^{2+} adsorbed and Mg^{2+} desorbed). Further support that cation exchange is the main geochemical process for Mg^{2+} enrichment was found in a laboratory column experiment where local groundwater was displaced by DSW [Ronen-Eliraz *et al.*, 2017]. Note that the observed $[\text{Mg}^{2+}]$ profile decreases gradually with time, reaching almost zero concentration at all depths (except 3 m) by the end of the January-February 2016 MAR event, which implies that the exchangeable Mg^{2+} at depths 0 to 3 m is already mostly depleted. Cation exchange can also explain some of the increase of $[\text{Na}^+]$, as the high $[\text{Ca}^{2+}]$ in the DSW (in comparison to all other cations in this water) can also be exchanged with adsorbed

Na^+ . However, some of the increase in $[\text{Na}^+]$ at the unsaturated zone is associated with an increase in $[\text{Cl}^-]$, and therefore assumed to be controlled also by evaporation (the high $[\text{Cl}^-]$ and $[\text{Na}^+]$ after the summer, measured on 12 January 2016, supports this assumption; see Figure 4a).

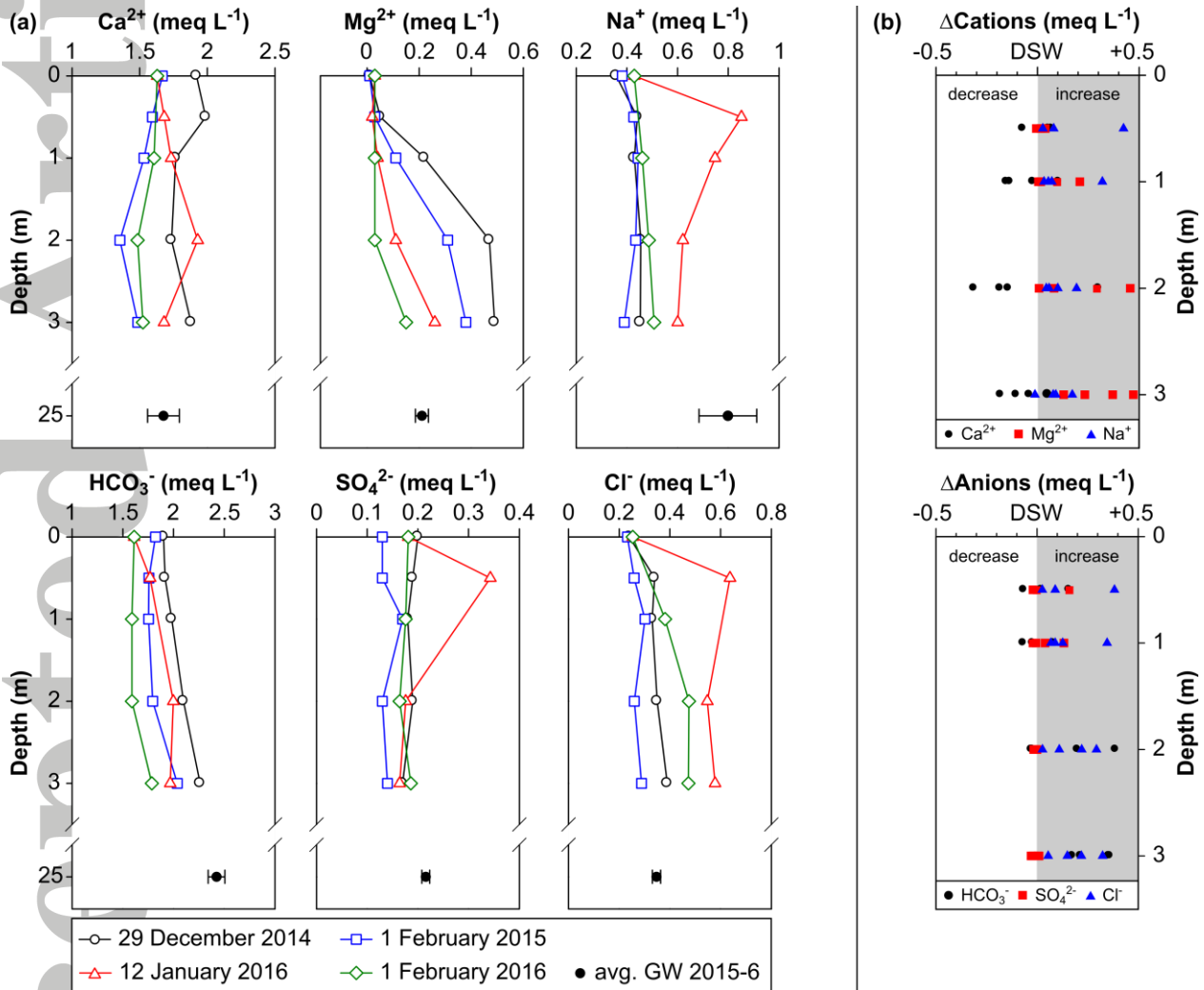


Figure 4. (a) Depth profiles of major ions during 2015 and 2016 MAR events. Depths 0–3 m is the variably-saturated zone that was sampled by suction cups. Average results of the groundwater observation wells OA and OB are shown at depth of 25 m (both perforated along depths of 20 to 30 m); note the break on the vertical axis. (b) The difference of major cations (top) and anions (bottom) relative to the DSW at the variably-saturated zone (positive or negative difference indicate an increase or decrease in ion concentration, respectively).

The solute concentration of the major ions in the shallow groundwater (observation wells OA and OB) is similar compared to the DSW for $[\text{Ca}^{2+}]$, $[\text{SO}_4^{2-}]$ and $[\text{Cl}^-]$, with some increase in $[\text{Mg}^{2+}]$, $[\text{Na}^+]$ and $[\text{HCO}_3^-]$ (at 25 m depth; Figure 4a). Comparing the stable water isotopes of the DSW ($\delta^{18}\text{O}$ between 1.2 to 1.4‰ and $\delta^2\text{H}$ between 10.4 to 11.3‰) with those of the shallow groundwater ($\delta^{18}\text{O}$ between 1.1 to 1.5‰ and $\delta^2\text{H}$ between 10.2 to 11.3‰) clearly demonstrates that the shallow groundwater at the observation wells OA and OB is practically enriched DSW. In contrast, the production wells at the Menashe site shows a distinct difference in the water isotope composition ($\delta^{18}\text{O}$ between -5.4 to -4.3‰ and $\delta^2\text{H}$ between -22.7 to -16.7‰). A summary of the water quality that was studied in this work is given in Table 1.

Ion enrichment occurs during infiltration of DSW along the variably-saturated zone by water-sediment interactions, and therefore controlled by the chemical composition of both the sediment and the source water. The concentrations of the major ions in the shallow groundwater are within the range of the unsaturated zone observations (with the exception of $[\text{HCO}_3^-]$), which indicates that the ion enrichment occurs already at the upper part of the unsaturated zone. The observed increased $[\text{HCO}_3^-]$ at the shallow groundwater is probably due to elevated $[\text{CO}_{2(g)}]$ and carbonate dissolution.

It is of importance to estimate the long-term impact of MAR with DSW on groundwater composition as well as on the sediment composition. Specifically, we are interested in the use of soft DSW (i.e., without the addition of calcium carbonate as post-treatment) for soil-aquifer-treatment (SAT) as an alternative post-treatment practice. An additional interest stems from the long-term enrichment of $[\text{Mg}^{2+}]$, since the deficiency of Mg^{2+} in DSW is a concern in Israel, because Mg^{2+} is considered essential for human health and agricultural irrigation [e.g., *Lehmann et al.*, 2016]. For this purpose, we formulate a reactive transport model, which is constrained to the above field observations.

Table 1. Water quality at the MAR Menashe site. DSW is desalinated seawater and GW is groundwater.

Parameter	Unit	GW production wells 2014 avg. (std.)	Shallow GW monitoring wells 2014-6 avg. (std.)	DSW inlet pipe 2014-16 avg. (std.) ^a	DSW recharge pond 2015 avg. (std.) ^b	DSW suction cups 2015-6 avg. (std.)
Ca	mg L ⁻¹	92.0 (13.0)	41.1 (11.4)	34.7 (2.3)	37.7 (0.2)	32.7 (3.9)
Mg	mg L ⁻¹	13.1 (2.7)	3.13 (0.89)	0.17 (0.08)	0.29 (0.02)	3.16 (2.92)
Na	mg L ⁻¹	36.4 (8.5)	20.7 (4.1)	8.4 (1.1)	11.5 (0.1)	11.2 (3.1)
K	mg L ⁻¹	1.46 (0.27)	0.83 (0.47)	0.30 (0.13)	0.4 (0.0)	0.80 (0.42)
HCO ₃	mg L ⁻¹	242 (28)	174 (35)	107 (7)	109 (1)	116 (13)
Cl	mg L ⁻¹	73.7 (19.8)	13.3 (1.4)	7.8 (1.4)	14.8 (0.4)	12.7 (5.0)
SO ₄	mg L ⁻¹	28.9 (8.0)	12.5 (2.8)	9.5 (2.1)	9.0 (0.1)	10.1 (3.0)
NO ₃	mg L ⁻¹	30.0 (9.2)	0.39 (0.32)	<0.25	<0.25	0.97 (1.43)
SiO ₂	mg L ⁻¹	11.0 (1.4) ^c	6.0 ^c	n/a	n/a	n/a
pH		7.35 (0.18)	7.78 (0.24)	7.76 (0.22)	7.74 (0.04)	7.92 (0.23)
EC	μS cm ⁻¹	694 (103)	285 (49)	186 (22)	193 (3)	226 (65)
Temp.	°C	20.9 (1.7)	22.6 (2.9)	23.4	18.9	20.6 (4.1)
δ ¹⁸ O	‰	-4.50 (0.02)	1.25 (0.15)	1.38 (0.05)	n/a	1.37 (0.10)
δ ² H	‰	-18.40 (0.05)	10.72 (0.39)	11.22 (0.17)	n/a	11.12 (0.54)

^aWater samples were taken before entering the recharge pond.

^bWater samples were taken during infiltration from the south, center and north parts of the recharge pond on 21 January 2015.

^cSiO₂ results were sampled in March 2017.

4 Reactive transport modeling

4.1 Model description

4.1.1 Flow model

The variably-saturated flow model, which is based on previous work [Ganot *et al.*, 2017] provides the flow field for the reactive transport model, and it is shortly described here for clarity. The flow model domain consists of 10 layers within the top 0–30.5 m of the sediment with 8 different hydraulic-characteristics that were based on the analyses of the sediment samples. The domain was discretized into 1000 elements of 0.1–4 cm thick (average of 3 cm). The van Genuchten–Mualem model [van Genuchten, 1980; Mualem, 1976] was used for the water retention curves and unsaturated hydraulic conductivity functions of the different sediments. The hydraulic parameters were obtained from measured particle size distribution and bulk density using Pedotransfer functions [Schaap *et al.*, 2001], and further model calibration. Average saturated hydraulic conductivity is 7.4 m/d, ranging between 0.1 and 13 m/d. Flow boundary conditions at the pond ground surface (top) are the ponding depth (monitored at its surface when filled) and no flow when the pond is empty. The bottom boundary is groundwater head (measured in well OA). The initial conditions (water content) were obtained from field data and by running a simulation from September to December 2014 prior to the 2015 MAR event.

4.1.2 Reactive transport model

We use the variably-saturated reactive transport model UNSATCHEM, which allows modeling of water flow, solute transport and major-ion chemistry [Šimůnek *et al.*, 1996]. The geochemical model includes cation exchange and calcite dissolution/precipitation reactions. The reactive transport of the 7 major ions (Ca^{2+} , Mg^{2+} , Na^+ , K^+ , HCO_3^- , Cl^- and SO_4^{2-}) is described by the following advection-dispersion equation [Šimůnek *et al.*, 1996]

$$\frac{\partial \theta c_k}{\partial t} + \rho_b \frac{\partial \bar{c}_k}{\partial t} + \rho_b \frac{\partial \hat{c}_k}{\partial t} = \frac{\partial}{\partial z} \left(\theta D \frac{\partial c_k}{\partial z} - q c_k \right) \quad k = 1, 2, \dots, 7 \quad (1)$$

where θ is the volumetric water content [$\text{L}^3 \text{L}^{-3}$], c_k is the total dissolved concentration of the component k [M L^{-3}], \bar{c}_k is the total adsorbed concentration (exchangeable cations) of the component k [M M^{-1}], \hat{c}_k is the total concentration of the component k in minerals [M M^{-1}] (in

this study we only model calcite dissolution/precipitation), ρ_b is the bulk density of the medium [M L^{-3}], D is the dispersion coefficient [$\text{L}^2 \text{T}^{-1}$] and q is the volumetric flux [L T^{-1}]. The second and third terms on the left side of equation (1) are zero for conservative species (Cl^- and SO_4^{2-} in this work). The volumetric flux q is calculated by the flow model that was described above. The dispersion coefficient D is given by [Suarez and Šimůnek, 1997]

$$D = \alpha_L \frac{|q|}{\theta} + D_m \tau \quad (2)$$

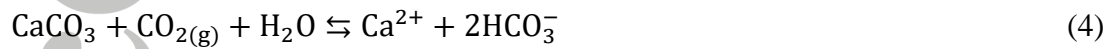
where α_L is the longitudinal dispersivity [L], D_m is the molecular diffusion coefficient in free water [$\text{L}^2 \text{T}^{-1}$] and τ is a tortuosity factor in the dissolved phase [-] defined as $\tau = \theta^{7/3} \theta_s^{-2}$ (Millington and Quirk [1961]; where θ_s is the saturated water content).

Cation exchange between aqueous and exchangeable phases is described using the Gapon equation, under the assumption that the CEC is constant [Suarez and Šimůnek, 1997]

$$K_{ij} = \frac{\bar{c}_i^{y+} (c_j^{x+})^{1/x}}{\bar{c}_j^{x+} (c_i^{y+})^{1/y}} \quad (3)$$

where k_{ij} is the Gapon selectivity coefficient, y and x are the valences of species i and j , respectively, \bar{c} is the concentration of the exchangeable cations (in $\text{meq kg}^{-1}_{\text{soil}}$), and c is the ion activity of the dissolved cations [-]. Three Gapon coefficients for cation pairs Mg/Ca, Ca/Na, and Ca/K are used in UNSTCHEM for the 4 major cations (Mg^{2+} , Ca^{2+} , Na^+ , and K^+). The Gapon selectivity coefficients in this study were optimized by inverse modeling as will be described in the next section.

Calcite precipitation and dissolution is described by the following equilibrium equations



$$k_{\text{sp}} = (\text{Ca}^{2+})(\text{CO}_3^{2-}) \quad (5)$$

where k_{sp} is the solubility product of calcite and parentheses represent ion activities. A detailed explanation of the carbonate system can be found in Suarez and Šimůnek [1997].

The reactive transport domain is based on the flow domain discretization but includes only 2 layers within 0–30.5 m depth in order to minimize the number of estimated parameters, as will be explained in the next section. Solute transport boundary conditions were concentration flux (Cauchy) and zero concentration gradient (Neumann) at the top and bottom boundaries, respectively. Solute concentration measured before the MAR events at the observation wells OA and OB were used as initial solute concentration in the sediment profile (Table 2).

Table 2. Water composition as inserted into the reactive transport model. DSW is desalinated seawater and GW is groundwater at the shallow observation wells. Ion concentration is in meq L⁻¹. DSW, shallow GW and Lake Kinneret were measured in this study.

Water type	Ca ²⁺	Mg ²⁺	Na ⁺	K ⁺	HCO ₃ ⁻	SO ₄ ²⁻	Cl ⁻
DSW (top boundary)	1.74	0.01	0.49	0.005	1.75	0.23	0.34
Shallow GW (initial conditions)	2.85	0.35	1.13	0.036	3.51	0.33	0.41
Lake Kinneret (top boundary) ^a	4.18	2.86	2.08	0.076	5.80	0.48	2.79
Soft DSW (top boundary) ^b	0.005	0.008	0.353	0.003	0.111	0.002	0.255

^aLake Kinneret water was recharged only for 4-hours on 25 December, 2014 (beginning of 2015 MAR event).

^bSoft DSW [Kloppmann *et al.*, 2008a] is the DSW composition before post-treatment that was used in the prediction simulations, section 4.4.2.

4.2 Parameter estimation

The reactive transport parameters were estimated by inverse modeling and by sediment analysis. The longitudinal dispersivity α_L was estimated from continuous measurements of bulk soil electric conductivity (bulk EC) at depth of 3 m, during 4-hours flushing of the high EC, Lake Kinneret water with DSW, in the beginning of the 2015 MAR event [Ganot *et al.*, 2017]. The breakthrough curve was analyzed using CXTFIT [Van Genuchten and Parker, 1984; Toride *et al.*, 1995] with analytical solution to the deterministic, equilibrium advection–dispersion equation (Figure 5). The longitudinal dispersivity was estimated by assuming a homogenous soil (upper sand) and a conservative tracer under steady-state conditions. The estimated dispersivity was applied to the entire transport domain.

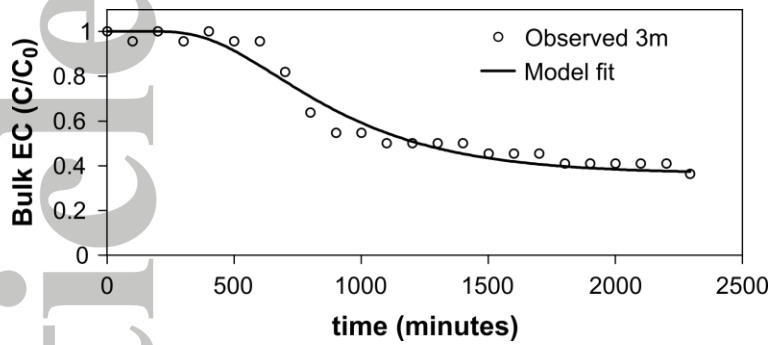


Figure 5. Observed and fitted breakthrough curve of bulk EC data during the MAR 2015 event when DSW flushes Lake Kinneret water. Y-axis is normalized concentration. The longitudinal dispersivity for the model was estimated by analysis of the breakthrough curve with CXTFIT.

The sediment parameters include bulk density, adsorbed exchangeable cations, calcite content and CEC that were measured, and $[\text{CO}_2]$ profile and Gapon selectivity coefficients that were estimated by calibration (Table 3). Initial calcite content was assumed equal to the measured carbonate content (Figure 2). The $[\text{CO}_2]$ along the sediment profile was considered increasing with depth [Walvoord *et al.*, 2005; Benavente *et al.*, 2010]. Field measurements of $[\text{HCO}_3^-]$ and pH (that together allow calculation of $[\text{CO}_2]$ through Henry's law constant) were only available from the upper sand and the shallow groundwater. Therefore, due to the lack of $[\text{CO}_2]$ field data, we assumed that the sediment $[\text{CO}_2]$ increases linearly with depth, using its slope as a fitting parameter that satisfies the $[\text{HCO}_3^-]$ field observations. The intercept of the linear $[\text{CO}_2]$ profile, located at the pond surface, was assumed to equal average atmospheric $[\text{CO}_2]$, 400 ppm.

The relatively low spatial resolution of field observations (i.e., lacking the 4 to 20 m interval) imposes some difficulty in optimizing the Gapon selectivity coefficients of each layer in the profile by inverse modeling. In addition, optimizing many parameters simultaneously in the variably-saturated zone may lead to a non-unique solution [Šimůnek and Hopmans, 2002]. Therefore, in order to simplify the reaction domain and to decrease the number of estimated parameters, it was divided into 2 sections (based on the available field observations): upper sand (0–4 m depth) and lower effective layer (4–30.5 m depth) which is a weighted average of all the underlying layers. Hence, the exchangeable cations, bulk density, and calcite content are all averaged values in the lower effective layer. The initially adsorbed cations in the lower layers (4–19 m depth) have relatively similar proportions and concentrations (Figure 2), which justify the effective layer simplification. This justification is weaker for the initial calcite content as the

measured calcite (carbonate) content along the sediment profile shows high variability (Figure 2). However, calcite reaction in the model is an equilibrium reaction that occurs mostly in the upper sand layer, and therefore the lower effective layer is also a reasonable simplification of the measured calcite content.

The simplified domain of two reactive layers reduces the Gapon selectivity coefficients that need to be optimized to four: $K_{Mg/Ca}$ and $K_{Ca/Na}$ for each of the two model layers ($K_{Ca/K}$ was not optimized because in all samples $[K^+] < 0.04 \text{ meq L}^{-1}$, rendering cation exchange with K^+ negligible). The Gapon selectivity coefficients were inversely estimated with UNSATCHEM and the optimization code UCODE [Poeter *et al.*, 2014], following Raij *et al.* [2016]. The optimized parameters in UCODE are obtained by minimizing iteratively the objective function [Hill, 1998]

$$S(\mathbf{b}) = \sum_{i=1}^n \omega_i [y_i - y'_i(\mathbf{b})]^2 \quad (6)$$

where $S(\mathbf{b})$ is the objective function, \mathbf{b} is a vector of estimated parameters, n is the number of observations, ω_i is the weight for the i th observation, y_i is the value of the i th observation and $y'_i(\mathbf{b})$ is the simulated value which corresponds to the i th observation using the parameters \mathbf{b} . A constant weight of one was used, as all observations were cations concentrations with an equal measurement error, on average.

Table 3. Parameters of the reactive transport model

Parameter	Value	Units	Source
Upper sand (0–4 m)			
Porosity	0.35		<i>Ganot et al.</i> [2017]
Bulk density (ρ_b)	1.56	g cm ⁻³	<i>Ganot et al.</i> [2017]
Cation exchange capacity	12.3	meq kg ⁻¹	this study
Initial adsorbed cations ($\overline{\text{Ca}}$, $\overline{\text{Mg}}$, $\overline{\text{Na}}$, $\overline{\text{K}}$)	4.7, 6.2, 1.1, 0.3	meq kg ⁻¹	this study
Initial calcite content	799	mmol kg ⁻¹	this study
Gapon coefficient Mg/Ca	2.1 (95% CI [1.39, 2.90])		this study
Gapon coefficient Ca/Na	0.12 (95% CI [0.03, 0.20])		this study
Lower effective layer (4–30.5 m)			
Porosity	0.32		<i>Ganot et al.</i> [2017]
Bulk density (ρ_b)	1.84	g cm ⁻³	<i>Ganot et al.</i> [2017]
Cation exchange capacity	92	meq kg ⁻¹	this study
Initial adsorbed cations ($\overline{\text{Ca}}$, $\overline{\text{Mg}}$, $\overline{\text{Na}}$, $\overline{\text{K}}$)	80.2, 9.6, 0.5, 1.7	meq kg ⁻¹	this study
Initial calcite content	1581	mmol kg ⁻¹	this study
Gapon coefficient Mg/Ca	0.34 (95% CI [0.29, 0.39])		this study
Gapon coefficient Ca/Na	5.33 (95% CI [4.35, 6.31])		this study
Both layers (0–30.5 m)			
Diffusion coefficient in water (D_m)	$3 \cdot 10^{-4}$	m ² d ⁻¹	<i>Šimůnek et al.</i> [1996]
Longitudinal dispersivity (α_L)	0.38 (95% CI [0.33, 0.43])	m	this study
[CO ₂] linear slope	19.7	ppm m ⁻¹	this study
Gapon coefficient Ca/K	0.05		<i>Vries and Posch</i> [2003]
Calcite solubility product (log k_{sp})	-8.38 (16 °C)		<i>Visscher and Vanderdeelen</i> [2012]

4.3 Calibration and validation

The observations from the 2015 and 2016 MAR events were used for calibration and validation, respectively. A total of 24 observation points of the cations Ca^{2+} , Mg^{2+} and Na^+ (12 in the variably-saturated zone and 12 in the shallow groundwater) were used for calibration, and 36 observation points for validation (24 in the variably-saturated zone and 12 in the shallow groundwater). The shallow groundwater samples were assigned to 25 m depth although the well screen is 10 m long (Figure 2). The 2015 MAR event was selected for calibration because the sediment attributes that are considered to be affected by the recharge (adsorbed cations and calcite content) were sampled prior to the 2015 event, during the drilling of the observation wells (August 2014), while similar sediment data are not available for the 2016 MAR event. The adsorbed cations and calcite content at the end of the calibration run were used as the solid-phase initial conditions for the validation run (i.e., the simulation was continuously run from the beginning of the MAR 2015 event to the end of the MAR 2016 event).

The modeled cations concentrations are in good agreement with the measured concentrations, with a root mean square error (RMSE) for the total cations of 0.055 and 0.157 meq L^{-1} for calibration and validation, respectively (Figure 6). Considering the RMSE of each individual cation in the validation (0.200, 0.081 and 0.164, corresponding to about 4, 1 and 4 mg L^{-1} , for Ca^{2+} , Mg^{2+} and Na^+ , respectively) provides an estimate of the model prediction error for a specific cation. The $[\text{HCO}_3^-]$ was excluded from the model RMSE since it was calibrated by fitting of the linear $[\text{CO}_2]$ profile. The simulated $[\text{HCO}_3^-]$ profile shows good fit for the calibration period, but underestimates $[\text{HCO}_3^-]$ in the upper sand during the validation period. This is because the $[\text{CO}_2]$ profile is assumed steady in the model, while in the field some variability of $[\text{CO}_2]$ and $[\text{HCO}_3^-]$ may exist (Figure 6b).

The 95% confidence intervals (CI) of the Gapon selectivity coefficients were used to evaluate the model sensitivity to these parameters. Simulations were made with the 16 possible combinations of the four Gapon selectivity coefficients, where each coefficient can take the value of the lower or upper bound of its 95% CI. The obtained maximum and minimum concentration values of each cation were used as the upper and lower limits of the model sensitivity range (Figure 6, in gray). Note that sensitivity analysis for the $[\text{HCO}_3^-]$ is not presented since it was calibrated by

fitting. The model sensitivity range for $[\text{Ca}^{2+}]$ and $[\text{Na}^+]$ is relatively wide, especially at depths where observations are absent, while the range for $[\text{Mg}^{2+}]$ is narrower. This suggests that the $[\text{Ca}^{2+}]$ and $[\text{Na}^+]$ are more sensitive to changes in the Gapon selectivity coefficients, compared to $[\text{Mg}^{2+}]$.

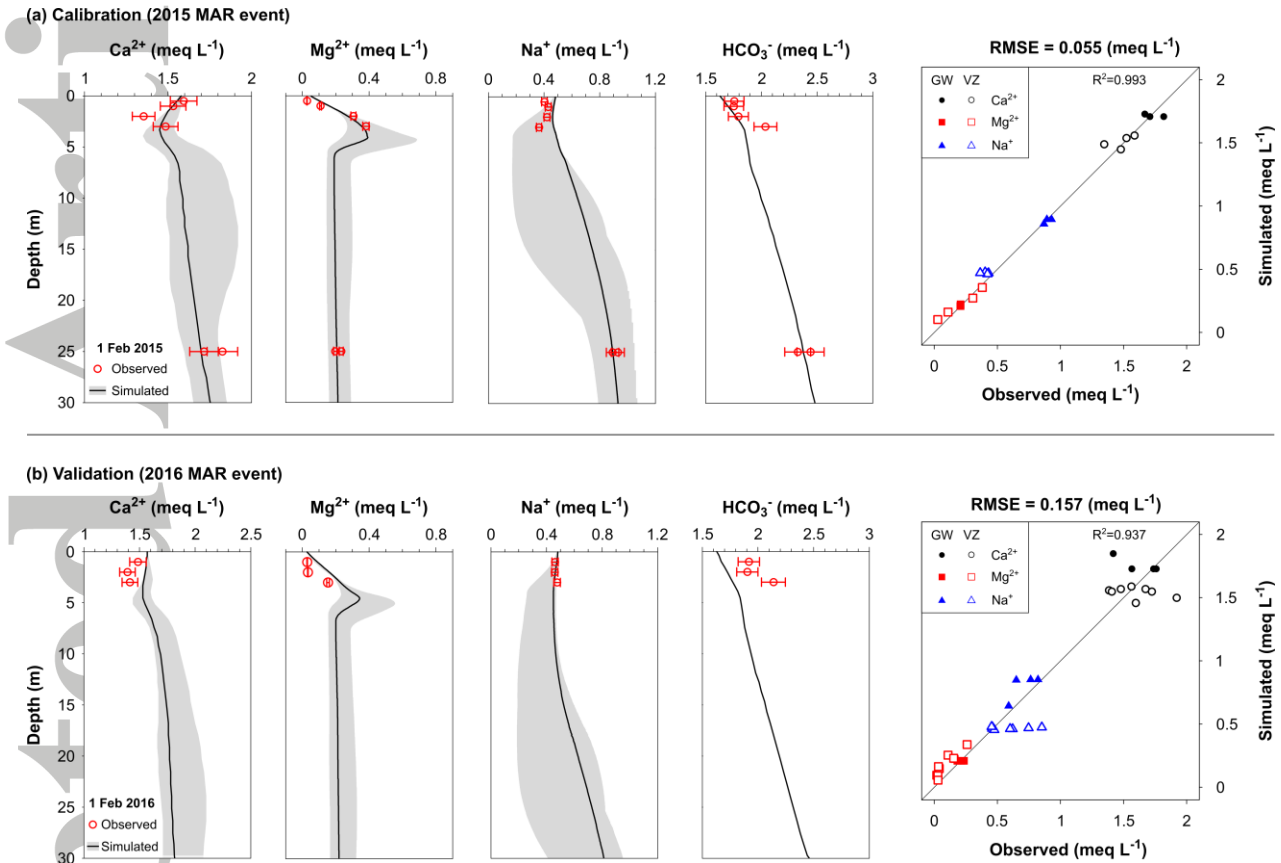


Figure 6. Observed and simulated ion concentrations. (a) calibration period (2015 MAR event) and (b) validation period (2016 MAR event). Model sensitivity due to the Gapon coefficients optimization is shaded in gray. Note that for the validation period, only observations measured on 1 February 2016 are shown in the ion concentration profiles. However, all the observed and simulated points are plotted in the RMSE graphs.

The simulated solid phase (exchangeable cations and calcite) before and after the two MAR events is shown in Figure 7. At the upper sand (0–4 m) Ca^{2+} is adsorbed while Mg^{2+} and Na^+ are desorbed, whereas at the top of the effective layer (4–7 m) Mg^{2+} is adsorbed, and Ca^{2+} and Na^+ are desorbed. At the end of MAR 2016, the initially low exchangeable Na^+ ($\bar{\text{Na}}$) is almost fully depleted along the effective layer (4–30.5 m). Note that the uncertainty of the Gapon exchange coefficient may lead to either adsorption or desorption of Na^+ in the upper sand, in contrast to the profiles of Ca and Mg that show a consistent trend (the sensitivity ranges in Figure 7 are

calculated similar to those in Figure 6). The calcite content profile is stable, indicating that no calcite has dissolved or precipitated, except for the uppermost part (0–4 cm depth) where calcite precipitated. This result shows that the lower effective layer simplification (4–30.5 m depth) is justified in the case of calcite. The obtained stable calcite content profile is reasonable as the Hadera desalination plant is obliged to supply DSW close to saturation with respect to calcite in order to meet the Israeli water quality standards.

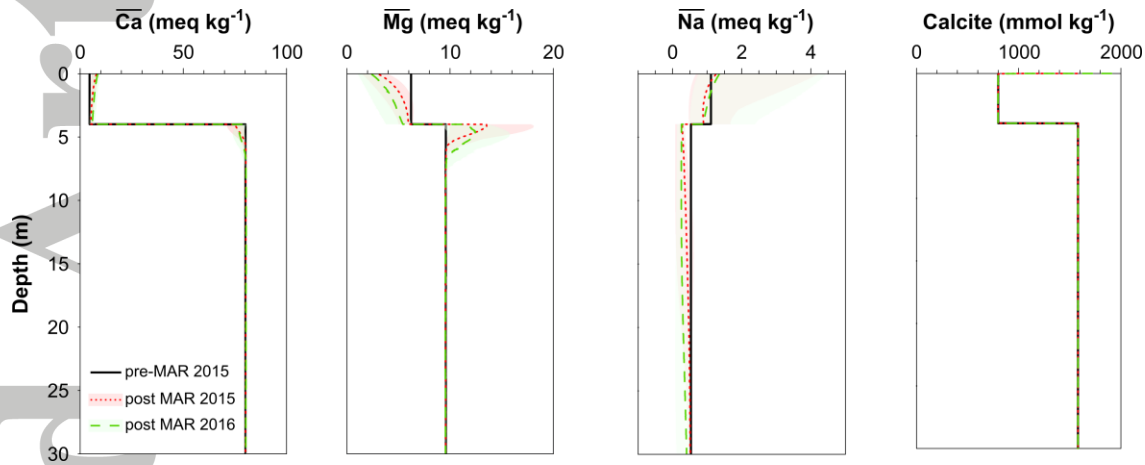


Figure 7. Simulated exchangeable cations and calcite concentration at the end of MAR 2015 and 2016 events. The pre-MAR 2015 profile (black line) is the solid-phase initial conditions of the calibration simulation; model sensitivity due to the Gapon coefficients optimization is shaded in light red and green.

The model results for the combined calibration and validation periods and the related field observations are shown in Figure 8 for the specific depths of 3 and 25 m. The high simulated cations concentration in the beginning of the 2015 MAR event is due to a 4-hours recharge ($\sim 2 \cdot 10^4 \text{ m}^3$) of Lake Kinneret waters ($\text{TDS} = 671 \text{ mg L}^{-1}$). This was followed by $\sim 2.45 \cdot 10^6$ and $\sim 1.3 \cdot 10^6 \text{ m}^3$ of DSW recharge, in 2015 and 2016, respectively. Overall, the model shows good agreement with the measured field observations. The exchange of Ca^{2+} for Mg^{2+} at the upper sandy layer is prominent from the adsorbed cations profiles of $\overline{\text{Ca}}$ and $\overline{\text{Mg}}$ (Figure 8a). Consequently, the $[\text{Ca}^{2+}]$ and $[\text{Mg}^{2+}]$ are always below and above the inlet DSW concentrations, respectively (see the arrows in Figure 8). At both depths of 3 and 25 m, changes in concentration occur during the MAR events, while the cations concentration is steady between the events. At 3 m depth the layer drains at the end of the MAR events (see the profile of the water content, θ) and therefore there is no ‘new’ DSW available for water-sediment interaction (the pore-water are in equilibrium with the sediment). On the other hand, at 25 m depth the sediment is always

saturated as water percolates through the variably-saturated zone (see θ profile in Figure 8b, and also water level in Figure 3b). However, the percolating water attains geochemical equilibrium with the sediment already at the upper part of the effective layer, as evident from the constant concentration of adsorbed cations at 25 m depth (Figure 8b). This explains the steady cations concentration between the MAR events at this depth, although this behavior might be an artifact of the lower layer simplification (4-30 m). The overestimation of $[\text{Ca}^{2+}]$ at 25 m depth at the end of the MAR 2016 event shows the model-validation highest deviation from observed concentration (0.4 meq L^{-1}). Comparison of the reactive-transport model with conservative-transport at 25 m depth (conservative in dashed line, Figure 8b) emphasizes the role of cation-exchange in controlling the dynamic concentration of the cations in the recharging water.

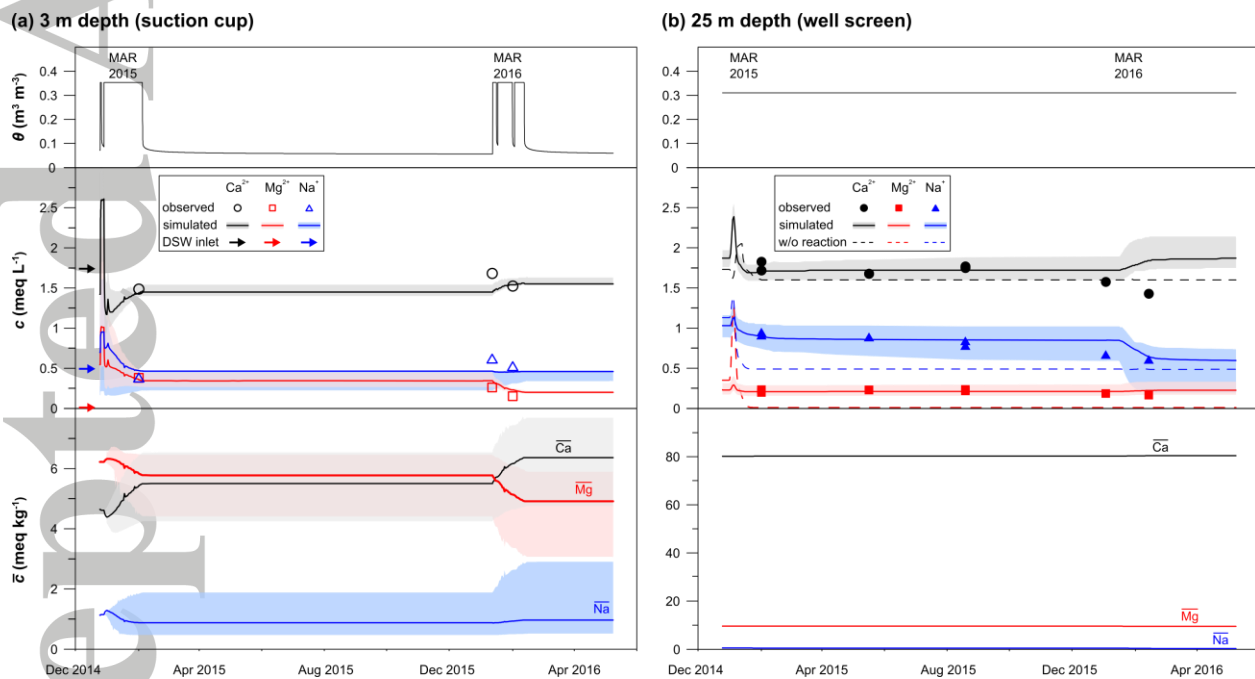


Figure 8. Simulation results of volumetric water content (θ), cations concentration (c) and adsorbed cations (\bar{c}) during the calibration and validation periods. (a) upper sand layer (3 m depth); (b) lower effective layer, at the well screen of the shallow groundwater (25 m depth). The dashed line is the results of a simulation without chemical reaction (given here for comparison). Model sensitivity due to the Gapon coefficients optimization is shaded in light gray, red and blue.

4.4 Predictions

Long-term predictions (50 years) of two scenarios of MAR with DSW (with and without post-treatment) were tested using the calibrated reactive transport model. Each year in the prediction simulation includes one month of continuous recharge of $\sim 2.5 \cdot 10^6 \text{ m}^3$ (based on the 2015 MAR event). Recharge is followed by groundwater fluctuations, which by the end of the year returns to the initial groundwater level, repeating this cycle for 50 years. Hence, solute and solid phase concentrations evolve during the prediction simulations while the hydraulic conditions of each year are simply repeated cycles. A total volume of $\sim 125 \cdot 10^6 \text{ m}^3$ is recharged after 50 years of MAR, corresponding to a total hydraulic load of $\sim 1100 \text{ m}$ of DSW (Table 4).

Table 4. Hydraulic loads and recharged volumes of the prediction simulations

Years	5	10	25	50
Hydraulic load (m)	110	220	550	1100
Recharged volume (10^6 m^3)	12.5	25	62.5	125

4.4.1 50 years of MAR with post-treated DSW

The simulation with post-treated DSW ($\text{TDS} = 160 \text{ mg L}^{-1}$) shows stable profiles of $[\text{Na}^+]$ and $[\text{HCO}_3^-]$ and a continuous cation exchange of Ca^{2+} for Mg^{2+} . This reaction is limited by the Mg^{2+} originally adsorbed to the sediment because the post-treated DSW provides unlimited supply of Ca^{2+} . Similar trends in the $[\text{Ca}^{2+}]$ and $[\text{Mg}^{2+}]$ profiles to those observed in the field just below the pond ground surface (Figure 4a), were recovered in the long-term simulation albeit deeper in the profile, because $[\text{Ca}^{2+}]$ is enriched and $[\text{Mg}^{2+}]$ is depleted (Figure 9a). Consequently, enrichment in $\overline{\text{Ca}}$ and depletion in $\overline{\text{Mg}}$ are evident, while the profiles of $\overline{\text{Na}}$ and calcite remain relatively stable (Figure 9b).

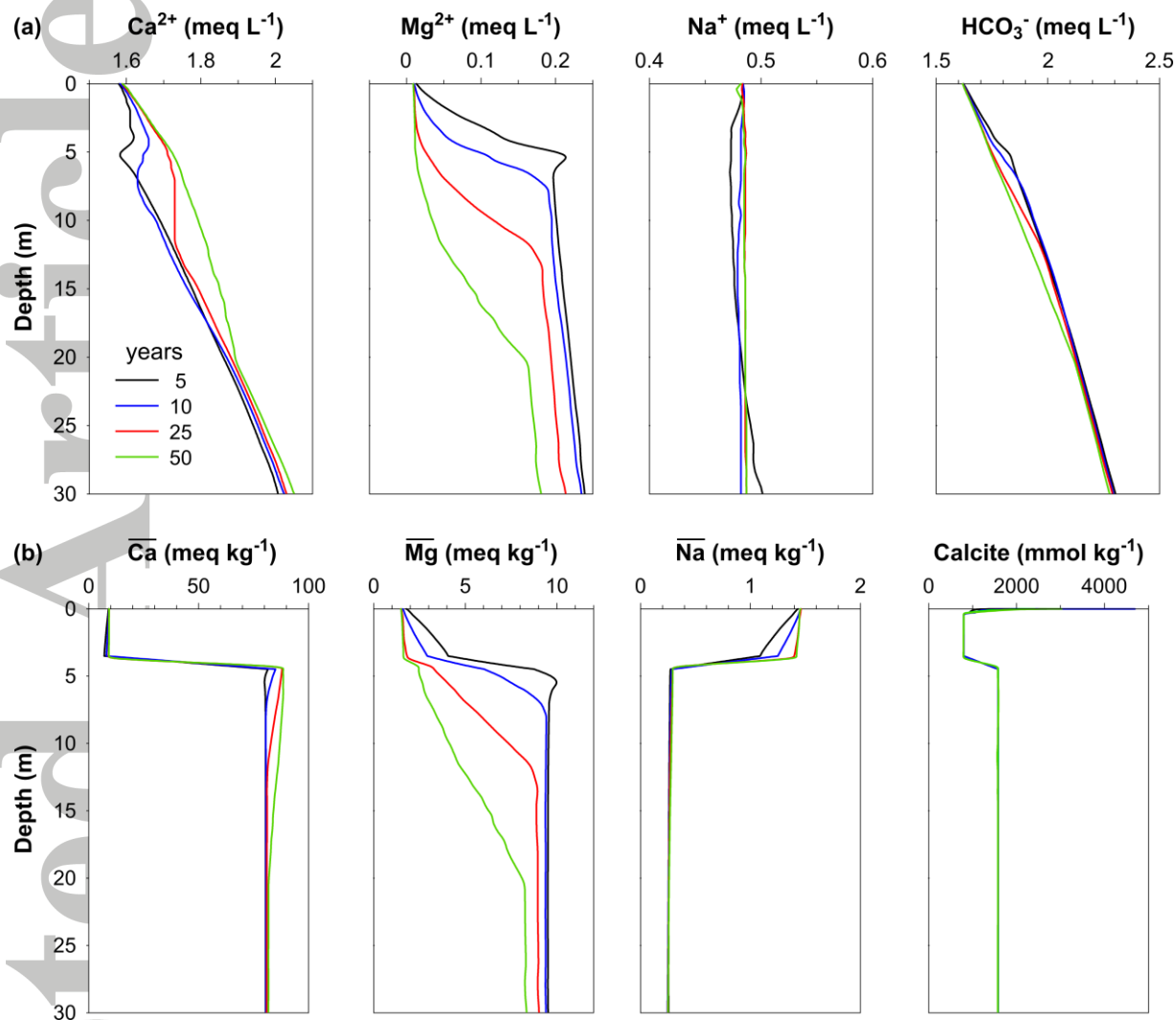


Figure 9. Simulated predictions for 50 years of MAR with post-treated DSW. (a) ion concentration along the sediment profile. (b) exchangeable (adsorbed) cations and calcite concentration along the sediment profile.

4.4.2 50 years of MAR with soft DSW

In the simulation using soft DSW (without post-treatment; TDS = 25 mg L⁻¹ with practically zero concentration of divalent ions), the profile of [Mg²⁺] is similar to the simulated prediction of DSW with post-treatment, whereas the profiles of [Ca²⁺], [Na⁺] and [HCO₃⁻] differ mainly in the upper part (Figure 10a). The enrichment in [Mg²⁺] depends on the exchange reaction with Ca²⁺. However, the soft DSW has negligible [Ca²⁺] such that calcite dissolution provides an alternative source for Ca²⁺. Hence, the exchange reaction depends on the dissolution reaction and is limited

by the calcite content in the sediment. This dependence is evident from a decrease in calcite content (Figure 10b) followed by a decrease in $[\text{Ca}^{2+}]$ and $[\text{HCO}_3^-]$ in the upper part of the sediment profile. The gradual decrease in $[\text{Ca}^{2+}]$ next to the pond ground surface (from 1.4 to 0.1 meq L^{-1} after 50 years) due to depletion of calcite content, promotes gradual increase in $\overline{\text{Mg}}$ and $\overline{\text{Na}}$ (i.e., adsorption of Mg^{2+} and Na^+ is preferred when $[\text{Ca}^{2+}]$ is low).

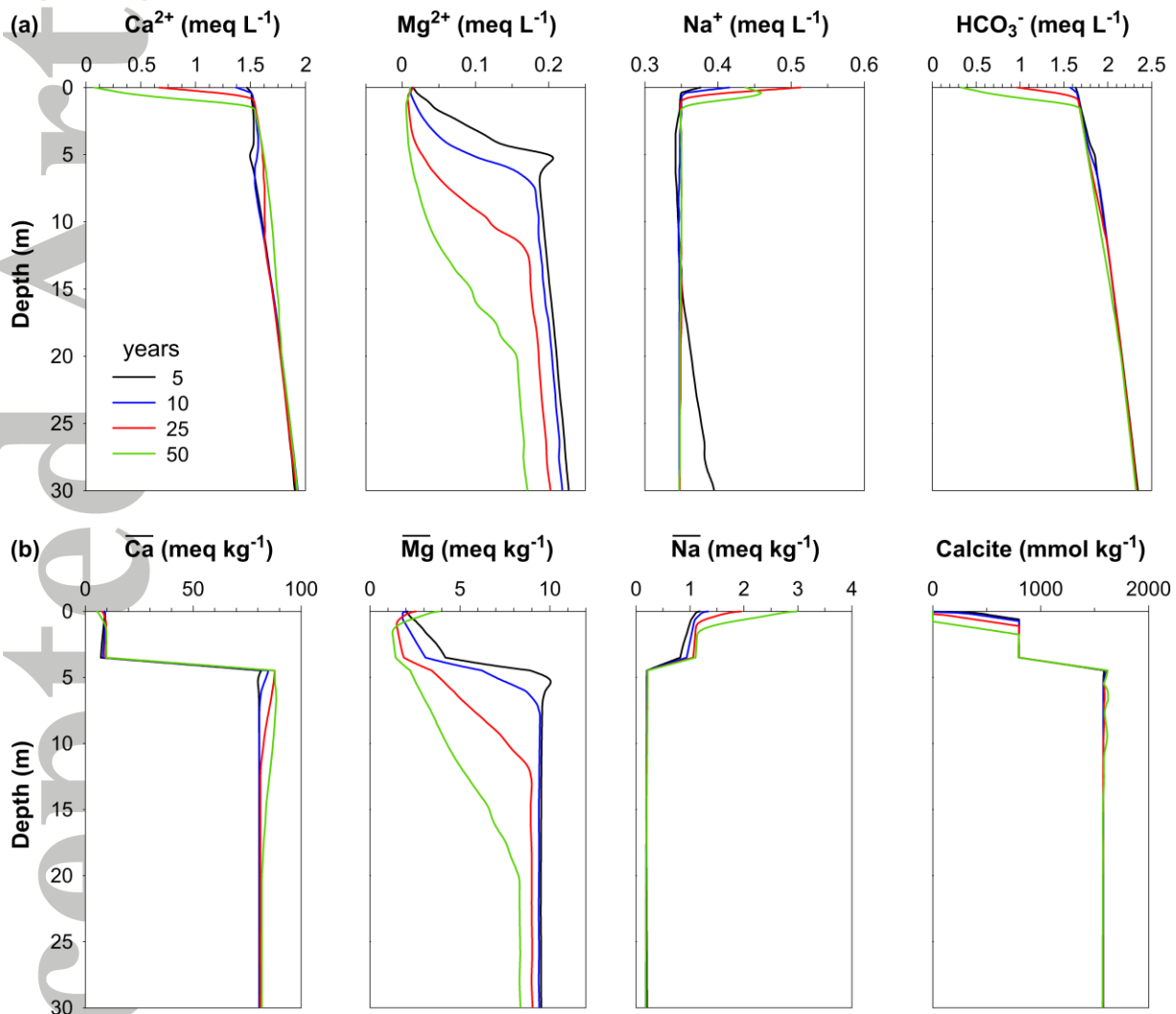


Figure 10. Simulated predictions for 50 years of MAR with soft DSW (without post-treatment). (a) ion concentration along the sediment profile. (b) exchangeable (adsorbed) cations and calcite concentration along the sediment profile.

5 Discussion

The predictive long-term simulations demonstrate the potential of using SAT through pond infiltration as a post-treatment (remineralization) for soft DSW. Both scenarios, with and without post-treatment, provide a relatively constant (and similar) water quality, which complies with the Israeli standards for desalinated water [Lahav and Birnhack, 2007] (Figure 11a). Hence, infiltrating soft DSW for MAR in the Menashe site can reduce the post-treatment costs ($3 \cdot 10^4$ kg of limestone per day from quarry; acid and base reagents), while complying with the water quality standards. However, we note that the hydraulic capacity of the specific MAR site limits the volumes that can be treated with this practice; for example, it cannot be used to treat the whole volume of DSW currently produced by the Hadera desalination plant (~ 130 million m^3 per year) in the Menashe site.

In Israel, DSW reached 60% of the domestic and industrial fresh water supply, and in some regions it is the only water supply year-round. Despite a decision by the Israeli Ministry of Health in 2009 to follow the recommendation by the World Health Organization (WHO) of a minimum of 10 mg L^{-1} [Mg^{2+}], for crop irrigation and public health considerations, it is still not enforced—to date, the Israeli standards for desalinated water have no criterion for Mg^{2+} [Birnhack *et al.*, 2011]. Therefore, the addition of Mg^{2+} is currently not included in the post-treatment stage at the Israeli desalination plants. Our simulations show an enrichment in [Mg^{2+}] during MAR with DSW in the variably-saturated zone ($\sim 2.5 \text{ mg L}^{-1}$, for both scenarios); while this falls below the WHO guidelines, it is higher than the current [Mg^{2+}] output of the Israeli desalination plants, which is practically zero. The enrichment in [Mg^{2+}] decreases during 50 years of MAR (from ~ 3 to $\sim 2 \text{ mg L}^{-1}$), because of its dependence on the $\overline{\text{Mg}}$ content in the sediment (Figure 11b). After 50 years, both scenarios predict an increase of the total sediment content of $\overline{\text{Ca}}$ by 3%, while $\overline{\text{Mg}}$ and calcite decrease by $\sim 23\%$ and $< 1\%$, respectively (Figure 11c). The small decrease in calcite content suggests that enrichment by infiltration of soft DSW can be a sustainable MAR practice at the Menashe site.

In this work we assumed that cation exchange is the main mechanism for Mg^{2+} enrichment based on the results of the column experiment by Ronen-Eliraz *et al.* [2017] and our field observations. Other sources for Mg^{2+} enrichment are probably minor. Generally, the magnesium (Mg)

concentration in the upper sediment profile of the Israeli Coastal Aquifer is lower than 0.2%, found mainly as low-Mg calcite, while dolomite is absent [Buchbinder & Friedman, 1980]. The SiO_2 in the shallow groundwater monitoring wells (Table 1) is due to an exchange process [Russak *et al.*, 2015; Stuyfzand, 1998; Wood & Signor, 1975], which negates Mg^{2+} enrichment by silicates dissolution. The dissolution of low-Mg calcite (assuming it exists) from the Kurkar is negligible because it depends on calcite dissolution which is limited during MAR of post-treated DSW (that are saturated with respect to calcite). However, for the soft DSW scenario, our simulation shows a 1% decrease in calcite content after 50 years (Figure 11c). Assuming this dissolved calcite contains ~1% Mg, we calculate $[\text{Mg}^{2+}]$ of ~1 mg L^{-1} in the shallow groundwater due to dissolution of low-Mg calcite, which, unfortunately together with the 2–3 mg L^{-1} from cation exchange will still be below the WHO guidelines for drinking water quality.

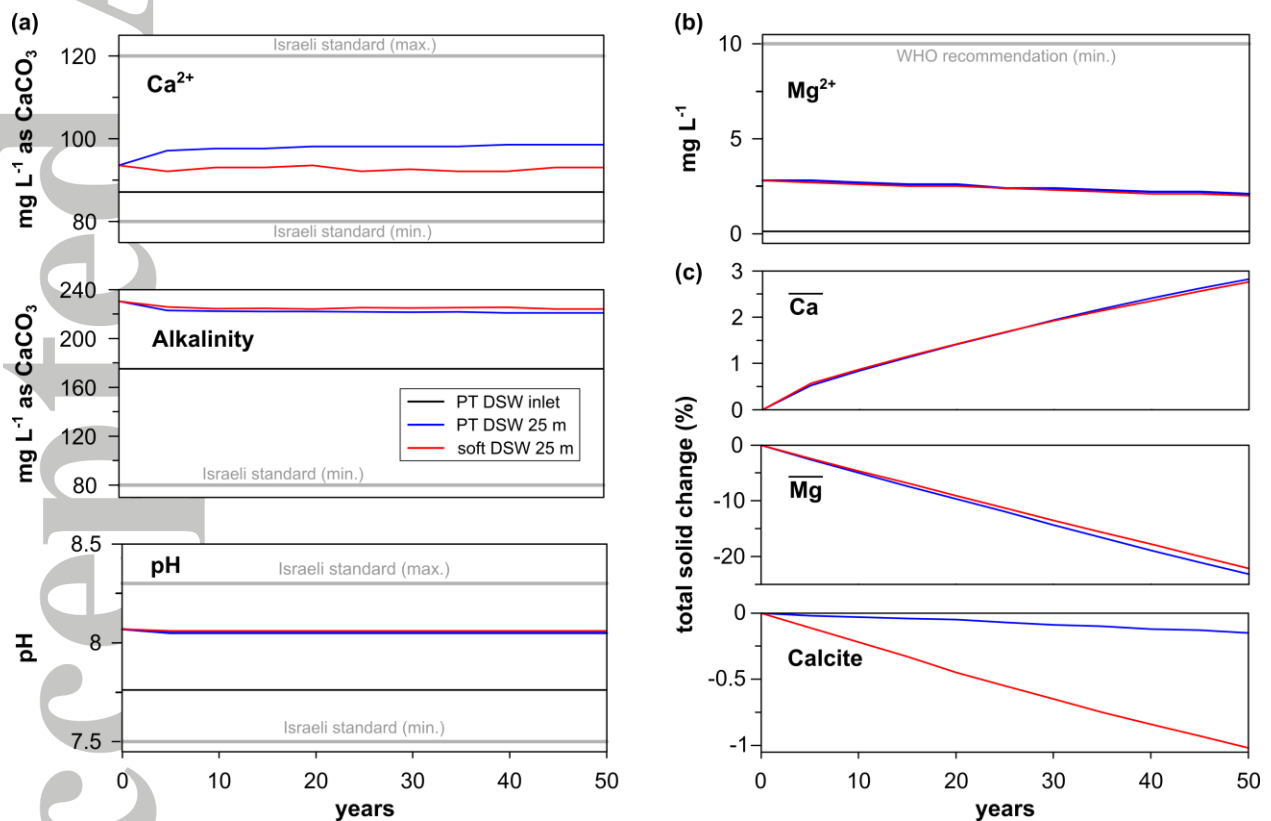


Figure 11. (a) Ca^{2+} , alkalinity and pH concentrations in the shallow groundwater (25 m depth) from the prediction simulations with post-treatment (PT) and without (soft), compared with the Israeli water quality standards for desalinated water (gray lines). Inlet DSW with PT is also shown for reference. (b) Mg^{2+} concentration in the shallow groundwater (25 m depth) compared with the recommendation of the World Health Organization (WHO). (c) Total change in percentage of the solid phase $\overline{\text{Ca}}$, $\overline{\text{Mg}}$ and calcite (positive indicate an increase) integrated along the model domain (30.5 m depth).

A depletion of calcite in the upper profile was recently reported for MAR using low TDS ($< 50 \text{ mg L}^{-1}$) reverse-osmosis wastewater (St-André site, Belgium; *Vandenbohede et al.* [2013]). Both their simulation and field observation show a substantial reduction in calcite content (73% in the first upper meter) during 10 years of MAR operation. The authors predicted that complete dissolution of calcite in the aquifer requires ~ 2600 years. In the Menashe site studied here, high carbonate content along the variably-saturated zone due to the Kurkar sediments (calcareous sandstone), leads to a prediction of 5000 years for complete dissolution of calcite along the variably-saturated zone. This prediction is based on our simulation with soft DSW, assuming a constant decrease in calcite content (see calcite profile in Figure 11c).

It should be noted that the water quality predictions in this study are restricted to the shallow groundwater just below the pond (3 m AMSL) after it has infiltrated through the variably-saturated zone. We do not model here the water quality of the production wells in deeper aquifer layers (-35 m AMSL, on average); this is because these wells are situated up to ~ 1 km from the infiltration ponds (see Figure 1), rendering their modeling beyond the scope of this paper.

Transport and reaction during DSW migration through the aquifer to the production wells, and its impact on water quality, are however of great interest, and therefore the subject of an ongoing study. Evidence for significant variability of ion concentration with depth in this coastal aquifer was provided by multilevel sampling conducted in a special observation well in Tel Aviv (~ 50 km to the south). Analysis showed that concentrations of all major ions in deeper production layers differ significantly from those in the shallow groundwater. Specifically, $[\text{Mg}^{2+}]$ increases dramatically from shallow to deep layers in that site [*Kurtzman et al.*, 2012].

6 Conclusions

The geochemical evolution during managed aquifer recharge (MAR) with reverse-osmosis desalinated seawater (DSW) at the Menashe site, in the Israeli Coastal Aquifer, was studied by in-situ field sampling and reservoir simulation. Field observations from both the unsaturated zone (0–3 m depth) and the shallow groundwater (~ 25 m depth) show that cation exchange is the dominant geochemical process, driven by the high Ca^{2+} concentration in the DSW (due to post-treatment that includes remineralization by calcite dissolution). Stable isotope analysis indicates that the composition of the shallow groundwater remains similar to the recharged DSW; however

it is enriched with Mg^{2+} due to cation exchange with Ca^{2+} , and with HCO_3^- and Ca^{2+} due to calcite dissolution. The ion enrichment is attained during infiltration of DSW through the variably-saturated zone.

The field observations were used to calibrate a variably-saturated reactive transport model. The calibrated model was used to simulate the geochemical evolution during 50 years of MAR with DSW (1 month of continuous infiltration per year), testing two optional scenarios in terms of water quality: (i) MAR with post-treated DSW ($\text{TDS} = 160 \text{ mg L}^{-1}$); and (ii) MAR with soft DSW ($\text{TDS} = 25 \text{ mg L}^{-1}$, with practically zero concentration of divalent ions). The two simulated scenarios resulted in relatively similar ion concentrations, albeit with a different Ca^{2+} enrichment mechanism (driving the cation exchange reaction). In the post-treated DSW scenario, Ca^{2+} is supplied with the inlet water due to remineralization at the desalination plant (the post-treatment process), while in the soft DSW scenario Ca^{2+} is supplied by calcite dissolution along the sediment profile. Our simulations predict for both scenarios a relatively stable Mg^{2+} enrichment at the shallow groundwater ($\sim 2.5 \text{ mg L}^{-1}$), improving upon the zero concentration currently found in the DSW supplied in Israel. Yet, this concentration is below the minimum Mg^{2+} concentration of 10 mg L^{-1} recommended by the World Health Organization. In terms of water quality, both scenarios are found within the range of the Israeli criteria for desalinated water. In terms of calcite content of the sediment, the soft DSW scenario predicts that its reduction is low ($<1\%$) along the variably-saturated profile, after 50 years (1100 m of infiltrating water). This suggests that using soil-aquifer-treatment as a remineralization technique for DSW is a potentially sustainable practice at the Menashe site and in other MAR sites with similar aquifer settings.

Acknowledgements

The research leading to these results received funding from the European Union Seventh Framework Program (FP7/2007-2013) under grant agreement # 619120 (Demonstrating Managed Aquifer Recharge as a Solution to Water Scarcity and Drought – MARSOL). We thank the Germany-Israel bi-national scientific cooperation BMBF-MOST, Project # WT1401 for partial funding of this work. Further thanks to Ido Nitzan (Volcani Center) for his technical assistance and Hagar Siebner (Ben-Gurion University) for the stable isotope analysis. We would also like to thank Prof. Dr. P. J. Stuyfzand and two anonymous reviewers for thorough and constructive review that improved the manuscript. The supporting information includes the data presented in this study.

References

- Al-Awadi, E., A. Mukhopadhyay, and A. J. Al-Haddad (1995), Compatibility Of Desalinated Water With The Dammam Formation At The Northwest Shigaya Water-Well Field, Kuwait – A Preliminary Study, *Hydrogeol. J.*, 3(4), 56–73, doi:10.1007/s100400050068.
- Benavente, J., I. Vadillo, F. Carrasco, A. Soler, C. Liñán, and F. Moral (2010), Air Carbon Dioxide Contents in the Vadose Zone of a Mediterranean Karst, *Vadose Zone J.*, 9(1), 126–136, doi:10.2136/vzj2009.0027.
- Birnhack, L., N. Voutchkov, and O. Lahav (2011), Fundamental chemistry and engineering aspects of post-treatment processes for desalinated water—A review, *Desalination*, 273(1), 6–22, doi:10.1016/j.desal.2010.11.011.
- Buchbinder, L. G., & Friedman, G. M. (1980). Vadose, Phreatic, and Marine Diagenesis of Pleistocene-Holocene Carbonates in a Borehole: Mediterranean Coast of Israel. *Journal of Sedimentary Research*, 50(2).
- Dillon, P. (2005), Future management of aquifer recharge, *Hydrogeol. J.*, 13(1), 313–316, doi:10.1007/s10040-004-0413-6.
- Ganot, Y., Holtzman, R., Weisbrod, N., Nitzan, I., Katz, Y., and Kurtzman, D. (2017). Monitoring and modeling infiltration–recharge dynamics of managed aquifer recharge with desalinated seawater. *Hydrol. Earth Syst. Sci.*, 21(9), 4479–4493. <https://doi.org/10.5194/hess-21-4479-2017>
- Gude, V. G. (2016), Desalination and sustainability – An appraisal and current perspective, *Water Res.*, 89, 87–106, doi:10.1016/j.watres.2015.11.012.
- Hill, M. C. (1998), Methods and guidelines for effective model calibration, *U.S. Geol. Surv. Water Resour. Invest. Rep.*, 98-4005.
- Israel Hydrological Service 2014: <http://www.water.gov.il/Hebrew/ProfessionalInfoAndData/DataHidrologeime/DocLib2/hydrological-report-sep14.pdf>, last access: 4 November 2016.
- Israel Meteorological Service: <http://www.ims.gov.il/IMS/CLIMATE/ClimaticAtlas>, last access: 16 June 2016.
- Kloppmann, W., A. Vengosh, C. Guerrot, R. Millot, and I. Pankratov (2008a), Isotope and Ion Selectivity in Reverse Osmosis Desalination: Geochemical Tracers for Man-made Freshwater, *Environ. Sci. Technol.*, 42(13), 4723–4731, doi:10.1021/es7028894.
- Kloppmann, W., E. Van Houtte, G. Picot, A. Vandenbohede, L. Lebbe, C. Guerrot, R. Millot, I. Gaus, and T. Wintgens (2008b), Monitoring Reverse Osmosis Treated Wastewater Recharge into a Coastal Aquifer by Environmental Isotopes (B, Li, O, H), *Environ. Sci. Technol.*, 42(23), 8759–8765, doi:10.1021/es8011222.
- Kurtzman, D., L. Netzer, N. Weisbrod, A. Nasser, E. R. Graber, and D. Ronen (2012), Characterization of deep aquifer dynamics using principal component analysis of sequential multilevel data, *Hydrol. Earth Syst. Sci.*, 16(3), 761–771, doi:10.5194/hess-16-761-2012.
- Lahav, O., and L. Birnhack (2007), Quality criteria for desalinated water following post-treatment, *Desalination*, 207(1–3), 286–303, doi:10.1016/j.desal.2006.05.022.
- Lehmann, O., O. Eckhaus, O. Lahav, and L. Birnhack (2016), Replenishing Mg(II) to desalinated water by seawater nanofiltration followed by magnetic separation of Mg(OH)₂(s)Fe₃O₄ particles, *Desalination Water Treat.*, 57(42), 19903–19916, doi:10.1080/19443994.2015.1107858.

- Levy, Y., Shapira, R. H., Chefetz, B., and Kurtzman, D. (2017). Modeling nitrate from land surface to wells' perforations under agricultural land: success, failure, and future scenarios in a Mediterranean case study. *Hydrol. Earth Syst. Sci.*, 21(7), 3811–3825. <https://doi.org/10.5194/hess-21-3811-2017>
- Loeppert, L. H., and D. L. Suarez (1996), Carbonates and gypsum, in *Methods of Soil Analysis–Part 3: Chemical Methods*, edited by S. L. Sparks *et al.*, pp. 437–474, *Soil Soc. of Am.*, Madison, Wis.
- Millington, R. J., and J. P. Quirk (1961), Permeability of porous solids, *Trans. Faraday Soc.*, 57, 1200, doi:10.1039/tf9615701200.
- Mualem, Y. (1976). A new model for predicting the hydraulic conductivity of unsaturated porous media. *Water Resources Research*, 12(3), 513–522. <https://doi.org/10.1029/WR012i003p00513>
- Mukhopadhyay, A., F. Szekely, and Y. Senay (1994), Artificial Ground Water Recharge Experiments in Carbonate and Clastic Aquifers of Kuwait, *JAWRA J. Am. Water Resour. Assoc.*, 30(6), 1091–1107, doi:10.1111/j.1752-1688.1994.tb03355.x.
- Mukhopadhyay, A., E. Al-Awadi, M. N. AlSenafy, and P. C. Smith (1998), Laboratory investigations of compatibility of the Dammam Formation Aquifer with desalinated freshwater at a pilot recharge site in Kuwait, *J. Arid Environ.*, 40(1), 27–42, doi:10.1006/jare.1998.0428.
- Mukhopadhyay, A., E. Al-Awadi, R. Oskui, K. Hadi, F. Al-Ruwaih, M. Turner, and A. Akber (2004), Laboratory investigations of compatibility of the Kuwait Group aquifer, Kuwait, with possible injection waters, *J. Hydrol.*, 285(1–4), 158–176, doi:10.1016/j.jhydrol.2003.08.017.
- Poeter, E., M. Hill, D. Lu, C. Tiedeman, and S. Mehl (2014), UCODE_2014, with new capabilities to define parameters unique to predictions, calculate weights using simulated values, estimate parameters with SVD, evaluate uncertainty with MCMC, and more, *Int. Ground Water Model. Cent. Rep. Appear.*
- Raij, I., J. Šimunek, A. Ben-Gal, and N. Lazarovitch (2016), Water flow and multicomponent solute transport in drip-irrigated lysimeters, *Water Resour. Res.*, 52(8), 6557–6574, doi:10.1002/2016WR018930.
- Ronen-Eliraz, G., A. Russak, I. Nitzan, J. Guttman, and D. Kurtzman (2017), Investigating geochemical aspects of managed aquifer recharge by column experiments with alternating desalinated water and groundwater, *Sci. Total Environ.*, 574, 1174–1181, doi:10.1016/j.scitotenv.2016.09.075.
- Russak, A., & Sivan, O. (2010). Hydrogeochemical Tool to Identify Salinization or Freshening of Coastal Aquifers Determined from Combined Field Work, Experiments, and Modeling. *Environmental Science & Technology*, 44(11), 4096–4102. <https://doi.org/10.1021/es1003439>
- Russak, A., Sivan, O., Herut, B., Lazar, B., & Yechieli, Y. (2015). The effect of salinization and freshening events in coastal aquifers on nutrient characteristics as deduced from column experiments under aerobic and anaerobic conditions. *Journal of Hydrology*, 529(Part 3), 1282–1292. <https://doi.org/10.1016/j.jhydrol.2015.07.034>
- Schaap, M. G., Leij, F. J., & van Genuchten, M. T. (2001). rosetta: a computer program for estimating soil hydraulic parameters with hierarchical pedotransfer functions. *Journal of Hydrology*, 251(3–4), 163–176. [https://doi.org/10.1016/S0022-1694\(01\)00466-8](https://doi.org/10.1016/S0022-1694(01)00466-8)
- Sellinger, A., and S. Aberbach (1973), Artificial recharge of coastal-plain aquifer in Israel, *Undergr. Waste Manag. Artif. Recharge*, 2.
- Shavit, U., and A. Furman (2001), The location of deep salinity sources in the Israeli Coastal aquifer, *J. Hydrol.*, 250(1–4), 63–77, doi:10.1016/S0022-1694(01)00406-1.

- Šimůnek, J., D. Suarez, and M. Šejna (1996), The UNSATCHEM software package for simulating one-dimensional variably saturated water flow, heat transport, carbon dioxide production and transport, and multicomponent solute transport with major ion equilibrium and kinetic chemistry, *Res Rep*, 141, 186.
- Šimůnek, J., and J. W. Hopmans (2002), Parameter optimization and nonlinear fitting, in *Methods of Soil Analyses*, edited by J. H. Dane, and G. C. Topp, pp. 139–158, *Soil. Sci. Soc. of Am.*, Madison, Wis.
- Suarez, D. L., and J. Šimůnek (1997), UNSATCHEM: Unsaturated water and solute transport model with equilibrium and kinetic chemistry, *Soil Sci. Soc. Am. J.*, 61(6), 1633–1646.
- Sumner, M. E., and W. P. Miller (1996), Cation Exchange Capacity and Exchange Coefficients, in *Methods of Soil Analysis Part 3—Chemical Methods*, pp. 1201–1229, Soil Science Society of America, American Society of Agronomy, Madison, WI.
- Stanhill, G., D. Kurtzman, and R. Rosa (2015), Estimating desalination requirements in semi-arid climates: A Mediterranean case study, *Desalination*, 355, 118–123, doi:10.1016/j.desal.2014.10.035.
- Stuyfzand, P.J., 1998. Quality changes upon injection into anoxic aquifers in the Netherlands: Evaluation of 11 experiments. In: Peters, J. (Ed.), *Proceedings of the 3rd International Symposium on the Artificial Recharge of Ground Water*, Amsterdam. A.A. Balkema, Rotterdam, pp. 283–291.
- Stuyfzand, P. J., E. Smidt, K. G. Zuurbier, N. Hartog, and M. A. Dawoud (2017), Observations and Prediction of Recovered Quality of Desalinated Seawater in the Strategic ASR Project in Liwa, Abu Dhabi, *Water*, 9(3), 177, doi:10.3390/w9030177.
- Toride, N., F. J. Leij, and M. T. van Genuchten (1995), The CXTFIT code for estimating transport parameters from laboratory or field tracer experiments, version 2.0, 121 pp., *U.S. Salinity Lab., U.S. Dep. of Agric.*, Riverside, Calif.
- van Genuchten, M. T. (1980). A Closed-form Equation for Predicting the Hydraulic Conductivity of Unsaturated Soils. *Soil Science Society of America Journal*, 44(5), 892.
<https://doi.org/10.2136/sssaj1980.03615995004400050002x>
- Van Genuchten, M. T., and J. Parker (1984), Boundary conditions for displacement experiments through short laboratory soil columns, *Soil Sci. Soc. Am. J.*, 48(4), 703–708.
- Vandenbohede, A., and E. Van Houtte (2012), Heat transport and temperature distribution during managed artificial recharge with surface ponds, *J. Hydrol.*, 472–473, 77–89, doi:10.1016/j.jhydrol.2012.09.028.
- Vandenbohede, A., E. V. Houtte, and L. Lebbe (2008), Groundwater flow in the vicinity of two artificial recharge ponds in the Belgian coastal dunes, *Hydrogeol. J.*, 16(8), 1669–1681, doi:10.1007/s10040-008-0326-x.
- Vandenbohede, A., E. Houtte, and L. Lebbe (2009a), Sustainable groundwater extraction in coastal areas: a Belgian example, *Environ. Geol.*, 57(4), 735–747, doi:10.1007/s00254-008-1351-8.
- Vandenbohede, A., E. V. Houtte, and L. Lebbe (2009b), Water quality changes in the dunes of the western Belgian coastal plain due to artificial recharge of tertiary treated wastewater, *Appl. Geochem.*, 24(3), 370–382, doi:10.1016/j.apgeochem.2008.11.023.
- Vandenbohede, A., I. Wallis, E. V. Houtte, and E. V. Ranst (2013), Hydrogeochemical transport modeling of the infiltration of tertiary treated wastewater in a dune area, Belgium, *Hydrogeol. J.*, 21(6), 1307–1321, doi:10.1007/s10040-013-1008-x.
- Visscher, A. D., and J. Vanderdeelen (2012), IUPAC-NIST solubility data series. 95. alkaline earth carbonates in aqueous systems. part 2. Ca, *J. Phys. Chem. Ref. Data*, 41(2), 023105–023105.

De Vries, W., and M. Posch (2003), Derivation of Cation Exchange Constants for Sand, Loess, Clay and Peat Soils on the Basis of Field Measurements in the Netherlands, *Alterra-Report 701*, 50 pp., *Alterra Green World Research*, Wageningen.

Walvoord, M. A., R. G. Striegl, D. E. Prudic, and D. A. Stonestrom (2005), CO₂ dynamics in the Amargosa Desert: Fluxes and isotopic speciation in a deep unsaturated zone, *Water Resour. Res.*, 41(2), n/a-n/a, doi:10.1029/2004WR003599.

Wood, W. W., & Signor, D. (1975). Geochemical factors affecting artificial groundwater recharge in the unsaturated zone. *Transactions of the ASAE*, 18(4), 677-0683.

Accepted Article